The structure of a dual-specificity tyrosine phosphorylation-regulated kinase 1A–PKC412 complex reveals disulfide-bridge formation with the anomalous catalytic loop HRD(HCD) cysteine

**Marina Alexeeva,‡ Espen Åberg,§ Richard A. Engh and Ulli Rothweiler***

Department of Chemistry, The Norwegian Structural Biology Centre, The Arctic University of Norway, 9037 Tromsø, Norway. *Correspondence e-mail: ulli.rothweiler@uit.no

Dual-specificity tyrosine phosphorylation-regulated kinase 1A (DYRK1A) is a protein kinase associated with neuronal development and brain physiology. The DYRK kinases are very unusual with respect to the sequence of the catalytic loop, in which the otherwise highly conserved arginine of the HRD motif is replaced by a cysteine. This replacement, along with the proximity of a potential disulfide-bridge partner from the activation segment, implies a potential for redox control of DYRK family activities. Here, the crystal structure of DYRK1A bound to PKC412 is reported, showing the formation of the disulfide bridge and associated conformational changes of the activation loop. The DYRK kinases represent emerging drug targets for several neurological diseases as well as cancer. The observation of distinct activation states may impact strategies for drug targeting. In addition, the characterization of PKC412 binding offers new insights for DYRK inhibitor discovery.

1. Introduction

A substantial body of evidence indicates that dual-specificity tyrosine phosphorylation-regulated kinase 1A (DYRK1A) is an important therapeutic target in neurological disorders, including the scourges of Alzheimer's disease (AD; Thies & Bleiler, 2012), Parkinson's disease (Kim *et al.*, 2006) and Huntington's disease (Kang *et al.*, 2005). The *dyrk1a* gene is located in the Down syndrome critical region (DSCR) on chromosome 21 (Guimerá *et al.*, 1996), and full or partial trisomy of DSCR in Down syndrome (DS) leads to over-expression of DYRK1A. This is coupled to mental retardation (Park *et al.*, 2009), along with an Alzheimer's-like dementia (Teipel & Hampel, 2006) that appears relatively early in life (compared with the occurrence of Alzheimer's disease in the general population). This occurs *via* several mechanisms (Liu *et al.*, 2008), one of which is the activity of DYRK1A to prime the tau protein for further phosphorylation by GSK-3β. This leads to the hyperphosphorylation of tau, followed by self-aggregation into neurofibrillary tangles, which are the primary biomarker of AD (Woods *et al.*, 2001). Further, DYRK1A has recently been identified as a risk factor for AD, enabling detection of the disease prior to the development of behavioural symptoms by analyzing human plasma (Janel *et al.*, 2014).

Parallel to studies of the pathophysiological roles of DYRK1A in neurological disorders, the structural mechanisms of DYRK catalysis and activation are coming under increasing scrutiny. DYRK1A, along with its analogues from

F238 gatekeeper
DFG motif
M240 hinge region
C312
C286
Y321
R328
R325
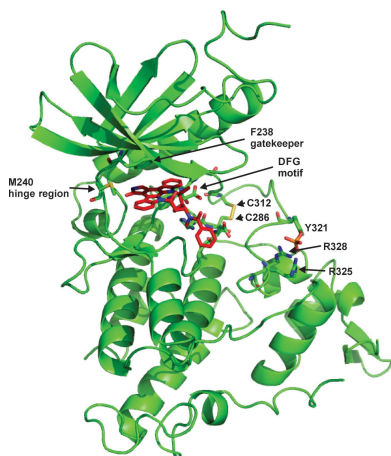
the evolutionarily conserved family of dual-specificity tyrosine phosphorylation-regulated kinases (DYRKs), belongs to the CMGC group in the human kinome (Manning *et al.*, 2002). The unique activity of the DYRKs, which gives the subgroup its name, is the dual capability to phosphorylate not only the serine/threonine residues within the consensus sequence (R*X*S/TR; Becker *et al.*, 1998) but also the second highly conserved tyrosine residue located on the activation segment in the Y*X*Y motif (Tyr321 in DYRK1A) during autoactivation (Becker & Sippl, 2011). Initially, the tyrosine phosphorylation was believed to be a one-time event that occurred during the translation of DYRK in the ribosome; more recent studies, however, have shown that DYRK1A is able to autophosphorylate other tyrosine residues and that it is not strictly coupled to the translation event (Walte *et al.*, 2013). The DYRK family is divided into two subclasses, class 1 (DYRK1A and DYRK1B) and class 2 (DYRK2, DYRK3 and DYRK4), based on sequence identity and the presence of specific sequence motifs (Becker *et al.*, 1998). The members of the DYRK family are regulators of diverse cellular processes, including cell division, differentiation, survival and apoptosis (Aranda *et al.*, 2011). The two DYRK1 isoforms (DYRK1A and DYRK1B) share 85% identity in the kinase domain. There is only one residue difference within the ATP-binding pocket, namely Met240 in DYRK1A *versus* Leu192 in DYRK1B at the gatekeeper +2 site of the hinge region. The role of DYRK1B has been investigated in myogenesis, and represents an emerging therapeutic target in pancreatic and ovarian cancers (Deng *et al.*, 2003; Friedman, 2010, 2013).

Besides their unique dual phosphorylation specificity, the DYRK kinases are distinguished by their idiosyncratic HCD sequence in the catalytic loop, which is otherwise highly conserved as HRD (Johnson *et al.*, 1996). The position of this cysteine creates the potential to form an intramolecular disulfide bridge with a cysteine from the activation loop (Soundararajan *et al.*, 2013; Becker & Sippl, 2011). A mechanistic role for such a disulfide bridge has not yet been demonstrated. However, redox regulation of proteins, including protein kinases, *via* the modification of cysteine residues is an important regulatory process in cell signalling (Eaton, 2006; Truong & Carroll, 2013). For example, the formation of an intramolecular disulfide bridge (not involving an HRD/HCD motif) in MKK6 and other MAP2Ks inactivates them by blocking ATP binding (Diao *et al.*, 2010).

The potential of DYRK1A as a drug target for DS, and advances in DYRK1A inhibitor programs aiming to treat cancer and Alzheimer's disease, have been summarized in recent reviews (Becker *et al.*, 2014; Smith *et al.*, 2012; Ionescu *et al.*, 2012). The inhibitors that have been crystallized in complex with DYRK1A are small molecules in the range 200–600 Da and belong to the ATP-competitive type I kinase inhibitors that bind to the active (DFG-in) conformation of the kinase domain (Anderson *et al.*, 2013; Ogawa *et al.*, 2010; Tahtouh *et al.*, 2012).

In this paper, we report a new crystal structure of DYRK1A in complex with the inhibitor PKC412, along with details of the binding of PKC412 to DYRK1A as characterized by

stability and activity assays. PKC412 (midostaurin) is a derivative of the broad-spectrum kinase inhibitor staurosporine, an alkaloid isolated from *Streptomyces staurosoreus* (Omura *et al.*, 1977), and has previously been described as a selective inhibitor of protein kinase C (PKC), VEGFR2, KIT, PDGFR and FLT3 (Fabbro *et al.*, 2000; Weisberg *et al.*, 2002). PKC412 is under investigation as a treatment for acute myeloid leukaemia (Fischer *et al.*, 2010; Stone *et al.*, 2012) and has been in phase III clinical trials since 2008 (ClinicalTrials, 2014).

2. Materials and methods

2.1. Expression and purification

DYRK1A and DYRK1B constructs comprising the kinase domain (DYRK1A, residues 126–490; DYRK1B, residues 78–451) were cloned into pEXP17 plasmid with N-terminal 6×His affinity tags and TEV protease cleavage sites. The proteins were expressed in shaker-flask cultures overnight at 17.8°C in TB medium. For the purification of DYRK1A, the cells were resuspended in a lysis buffer consisting of 50 m*M* sodium phosphate buffer pH 8.0 with 500 m*M* NaCl; for DYRK1B, 50 m*M* HEPES buffer pH 8.0, 50 m*M* KCl, 250 m*M* NaCl was used. The bacteria were lysed by sonication in the presence of 0.5% Tween 20. Purification was performed using Ni–NTA columns and an imidazole gradient (10–500 m*M*), followed by cleavage with TEV protease overnight and a second Ni–NTA column to separate the kinase from uncut protein and protease. Final purification of DYRK1A was performed by size-exclusion chromatography (SEC) in 50 m*M* MOPS pH 6.8, 50 m*M* KCl, 2 m*M* β-mercaptoethanol and that of DYRK1B was performed in 50 m*M* HEPES buffer pH 8.0, 50 m*M* KCl, 250 m*M* NaCl, 2 m*M* β-mercaptoethanol.

2.2. Crystallization

Screening for crystallization was performed with DYRK1A in 96-well sitting-drop plates, mixing 200 nl protein solution with 200 nl precipitant solution. Commercially available screens as well as in-house screens were used. An initial hit was found in the JCSG-plus screen (Molecular Dimensions) consisting of 0.2 *M* sodium thiocyanate, 20% PEG 3350. This condition was further optimized and improved by an additive screen with 96 conditions (Hampton Research), which produced the final crystallization condition: 10–16% PEG 3350, 0.1 *M* potassium thiocyanate, 0.1 *M* KCl (or 0.1 *M* NaCl or 0.1 *M* LiCl; other salts of alkali halides were also successfully used).

For co-crystallization with the inhibitor PKC412, the kinase DYRK1A was concentrated to 7–10 mg ml^{-1} in SEC buffer and mixed with inhibitor solution in DMSO to achieve an approximately threefold molar excess of inhibitor. The final concentration of DMSO was ~4%. The protein–inhibitor mixture was then mixed in a 1:1 ratio with the crystallization solution [100 m*M* potassium thiocyanate, 50–100 m*M* LiCl (or NaCl or KCl), 10–16% PEG 3350] to give a final drop size of 4 µl. Crystallization was performed in 24-well hanging-drop plates. Octahedron-shaped crystals appeared within 5–7 d at

Table 1
Crystallographic data and model statistics.

Values in parentheses are for the final shell.

Data collection	
Source	Beamline 14.1, BESSY II
Detector	Pilatus 6M
Wavelength (Å)	0.918
No. of crystals used	1
No. of frames	360
Oscillation range per frame (°)	0.5
Diffraction data	
Space group	$P2_12_12_1$ [No. 19]
Unit-cell parameters (Å)	$a = 87.8$, $b = 87.9$, $c = 229.9$
Protein molecules in asymmetric unit	4
No. of measurements	359740
Unique reflections	55625
Resolution range (Å)	48.3–2.6 (2.7–2.6)
Completeness (%)	99.7 (98.6)
Mosaicity (°)	0.2
$\langle I/\sigma(I) \rangle$	9.1 (1.9)
Observed R factor (%)	16.7 (104)
$CC_{1/2}$	99.4 (64.7)
Refinement	
Resolution limits (Å)	48.3–2.6 (2.7–2.6)
No. of reflections used	52841
Reflections observed (%)	99.7
Free reflections (%)	5.0
No. of protein atoms	11036
No. of heterogen atoms	176
No. of waters	223
R factor (overall/free) (%)	20.8/24.8
Overall figure of merit	0.87
Wilson B factor (Å^2)	46.8
R.m.s.d.	
Bonds (Å)	0.0064
Angles (°)	1.3
Ramachandran plot	
Favoured (%)	94.9
Allowed (%)	5.1
Outliers (%)	0

room temperature. Crystals were cryoprotected in crystallization solution modified to include 30% ethylene glycol and were flash-cooled in liquid nitrogen.

2.3. Structure solution and refinement

X-ray diffraction data were collected at the Helmholz Zentrum Berlin (Berlin Electron Storage Ring Society for Synchrotron BESSY II, Berlin, Germany). The images were integrated using the *XDSapp* software (Krug *et al.*, 2012) provided by the Helmholz Zentrum Berlin. The resolution cutoff chosen by the software is based on the $CC_{1/2}$ (Evans, 2012; Karplus & Diederichs, 2012). The structure was solved by molecular replacement with *Phaser* (McCoy *et al.*, 2007) using the DYRK1A structure with PDB code 3anq (Ogawa *et al.*, 2010) as a search model. Refinement was performed by iterative cycles of *PHENIX* (Adams *et al.*, 2010) and the *CCP*4 (Winn *et al.*, 2011) program *REFMAC*5 (Murshudov *et al.*, 2011) followed by the manual refitting of residues into the electron-density map using *Coot* v.0.7.2 (Emsley *et al.*, 2010). The cif file for PKC412 was generated by *PRODRG* (Schüttelkopf & van Aalten, 2004). Waters were placed by *Coot* v.0.7.2 (Emsley *et al.*, 2010). The crystallographic data and model statistics are summarized in Table 1.

2.4. Thermal shift assay

20 µl 1 mg ml^{-1} DYRK1A in SEC buffer was mixed with 5 µl SYPRO Orange solution and either 1 µl DMSO or inhibitor (PKC412 or harmine; 10 mM) in DMSO was added. Samples were heated from 10 to 90°C in 0.3°C steps and the melting point was calculated from the slope of the melting curve. Each experiment was performed as three replicates.

2.5. Activity assay

Determination of the enzyme activity, the K_m value for DYRK1A and DYRK1B and the inhibitory constants was performed by an ATP-regenerative NADH-consuming assay (Cook *et al.*, 1982). The enzyme velocity was measured at 340 nm over a time period of 300 s at room temperature. ATP and the peptide RRRFRPASPLRGPPK (DYRKtide) were used as substrates. For determination of the K_m, the reaction mixture was composed of 75 µl 100 mM MOPS buffer pH 6.8, 10 mM KCl, 10 mM MgCl, 1 mM phosphoenolpyruvate, 1 mM DYRKtide, 1 mM β-mercaptoethanol, 15 units ml^{-1} lactate dehydrogenase, 10 units ml^{-1} pyruvate kinase and 10.7 mM NADH. 10 µl 5–20 µM DYRK1A or DYRK1B and 10 µl ATP in the concentration range from 4 µM to 50 mM were added to give a total volume of 95 µl. For determination of the K_i, the
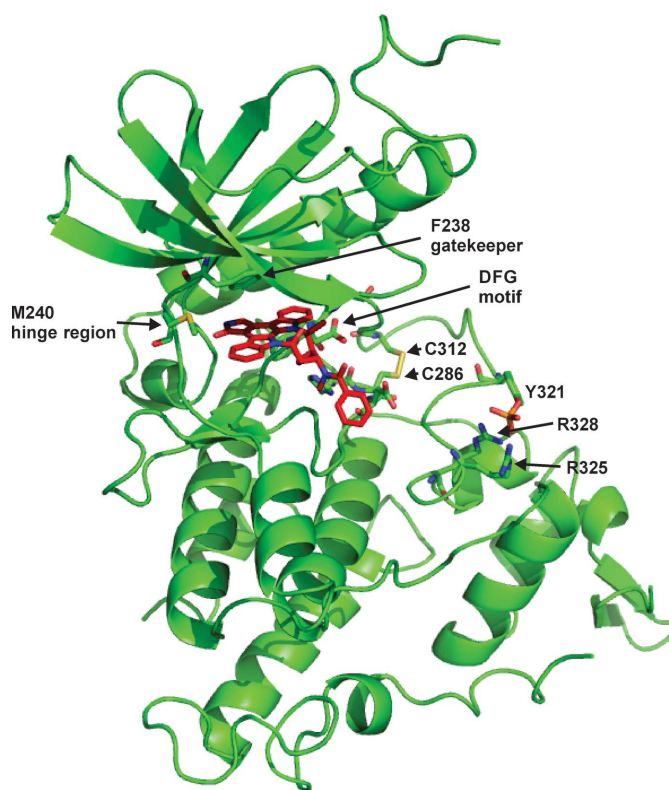

Figure 1
Overview of DYRK1A in complex with PKC412 (chain *A*) showing key features. The PKC412 inhibitor is shown as red sticks. Stick representations also highlight Met240 of the hinge, the gatekeeper Phe238, the DFG motif, the phosphotyrosine Tyr321 of the activation loop, its anchoring arginines Arg328 and Arg325, and the disulfide bridge between Cys286 and Cys312.

reaction mixture was used as described above but a constant concentration of 128 µM ATP was combined with 2 µl PKC412 in DMSO at concentrations ranging from 4 nM to 20 µM to give a total volume of 97 µl. All measurements were performed in triplicate at room temperature. The data were analyzed using *GraphPad Prism* 6.

3. Results

3.1. Overall crystal structure

The crystal structure contains a tetramer as the asymmetric unit, with the four individual DYRK1A molecules related to each other by three perpendicular twofold rotation axes (as previously described for PDB entries 3anq and 3anr; Ogawa *et al.*, 2010) and with the typical protein kinase fold also shared by DYRK structures (Ogawa *et al.*, 2010; Soundararajan *et al.*, 2013; Tahtouh *et al.*, 2012; Anderson *et al.*, 2013). Tyr321 in the activation segment is phosphorylated in the structure (Fig. 1) and is anchored to Arg325 and Arg328. The four individual chains in the asymmetric unit are not identical; chain *A* has the best fit to the electron density and is the most complete chain. The three other chains show more disorder, especially in the CMGC insert. Chain *A* lacks clear density in the loop comprised of amino acids 409–412, chain *B* lacks density for amino acids 213–218 and 407–414, chain *C* lacks density for amino acids 408–412 and chain *D* lacks density for amino acids 408–414 and 437–444.

3.2. Binding of PKC412

Contours for PKC412 were clearly visible in the difference electron-density map, and the fit is nearly unambiguous. One partial exception is the phenyl-ring terminus, especially for the inhibitor bound in chain *C*. PKC412 is bound in the ATP pocket *via* two hydrogen bonds made by the amine and ketone group in the 3-pyrroline-2-one head group of PKC412 to the hinge amino acids Glu239 and Leu241. Owing to the lack of any additional hydrogen acceptor or donor in the 3-pyrroline-2-one head group, there can be no polar interaction with the catalytic Lys188, in contrast to previous DYRK1A–inhibitor structures (Ogawa *et al.*, 2010), and the binding involves mostly buried hydrophobic surfaces (Fig. 2*a* and Supplementary Fig. S1). The phenyl-ring extension of PKC412 emerges from the ATP pocket, and has Glu291 as its closest neighbour (3.3 Å); the next neighbours Asn244 and Tyr246 are at a distance of greater than 5 Å. In contrast to staurosporine, PKC412 does not have an NH group that could make a stabilizing hydrogen bond to the carbonyl of Glu291, as seen, for example, in the PKA–staurosporine structure with PDB code 1stc (Glu170 in PKA numbering; Prade *et al.*, 1997). Its replacement, the benzoyl group, induces a rotamer shift that places the methyl group at the position of the former hydrogen bridge, displacing PKC412 upwards. On average, PKC412 binds protein kinases more weakly than staurosporine (Gani & Engh, 2010). The loss of this additional hydrogen bridge is likely to be a contributor to this.
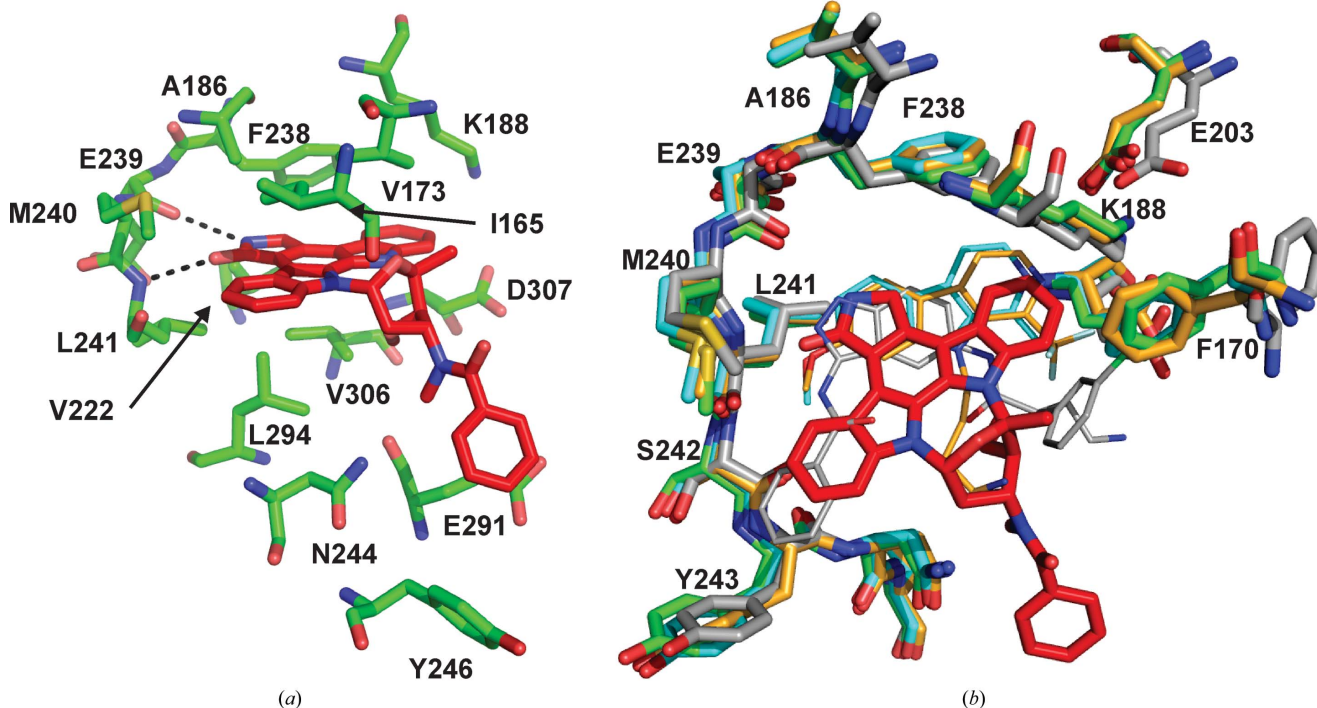

Figure 2
(*a*) Binding of PKC412 to DYRK1A. Hydrogen bonds are shared by the backbone atoms of Glu239 and Leu241. However, most of the interactions are *via* hydrophobic residues. The catalytic lysine (Lys188) does not participate in the binding of PKC412. (*b*) Overlay of different DYRK1A structures with inhibitors: harmine (PDB entry 3anr, cyan), LDN-211898 (PDB entry 5aik, orange), DJM2005 (PDB entry 2vx3, grey) and PKC412 (PDB entry 4nct, red).

One exception to the weaker binding of PKC412 compared with staurosporine is observed for MAP3K3 (or MEKK3). It binds PKC412 with a K_d of 210 nM, an increase of more than tenfold over that for binding to staurosporine (Davis *et al.*, 2011). As no structure of the kinase domain of MAP3K3 has been published, hypotheses for this increase remain speculative. If the binding data are correct, there may be no penalty for the loss of a hydrogen bond as described above, and in addition there must be MAP3K3-specific stabilizing interactions, presumably with the phenyl group of PKC412. The amino acids following the HRD (HCD in DYRK1A) segment might play a role in stabilization of the phenyl group of PKC412. Glu291 in DYRK1A (HCDLKPE291) corresponds to an alanine in MAP3K3 (HRDIKGA493), which would allow more space and possibly a different rotamer of PKC412, which might further allow the carbonyl moiety of PKC412 to form hydrogen-bonding interactions. This carbonyl group is oriented towards solvent in DYRK1A. Other amino-acid residues in MAP3K3 might directly interact with the phenyl ring of PKC412, adding a stabilizing effect. This ring has no rigidifying interactions in DYRK1A and is partially disordered. However, homology models for MAP3K3 (ProteinModelPortal; http://www.proteinmodelportal.org/query/uniprot/Q99759) do not identify any obvious candidates for such interactions.

The main target for the therapeutic effects of PKC412 is FLT3, to which PKC412 and staurosporine bind with a similar high potency (Davis *et al.*, 2011). One crystal structure is available for FLT3 (PDB entry 1rjb; Griffith *et al.*, 2004). This is in a DFG-out conformation, in which the phenylalanine would block the binding of PKC412 (or staurosporine) to the ATP-binding pocket. Indeed, PKC412 binds to FLT3 in its active conformation (as, for example, necessary to explain the pattern of resistance mutations that occur in FLT3; von Bubnoff *et al.*, 2009). However, as with MAP3K3 above, the identification of key structural features of FLT3 that would anomalously leave it unaffected by the factors that make PKC412 a weaker inhibitor compared with staurosporine for the majority of the kinases are not possible without further experimental information.

Several structures of DYRK1A with inhibitors have been published. An overlay of PKC412 (red) with harmine (PDB entry 3anr, cyan; Ogawa *et al.*, 2010), DJM2005 (PDB entry 2vx3, grey; Soundararajan *et al.*, 2013) and LDN-211898 (PDB entry 5aik, orange; J. M. Elkins, M. Soundararajan, J. R. C. Muniz, G. Cuny, J. Higgins, A. Edwards, C. Bountra & S. Knapp, unpublished work) (Fig. 2b) shows that the ATP-binding pockets are identical with the different inhibitors bound with one exception: the inhibitor DJM2005 induces a rotamer change for Phe170 of the glycine-rich loop. Although the inhibitors occupy roughly the same volumes, the additional hydrogen bonds of harmine and LDN-211898 to Lys188 are associated with deeper penetration into the ATP-binding pocket compared with PKC412 and DJM2005 (Fig. 2b). All of the inhibitors make hydrogen bonds to the hinge and the backbone carbonyl or amide groups of Glu239, Met240 and/or Leu241.

3.3. Disulfide bridge

A major distinguishing feature of the structure described here (PDB entry 4nct) is the disulfide bridge formed between Cys286 of the HCD motif in the catalytic loop and Cys312 in the activation segment (Supplementary Figs. S2 and S3). This disulfide bridge is present in all four monomers of the asymmetric unit. The distances between the two cysteine S atoms after refinement in chains *A*, *B*, *C* and *D* (without bond restraints) are at ideal distances for disulfide bridges (on average 2.1 Å). The previously published structure with PDB code 2vx3 (Soundararajan *et al.*, 2013), with a reduced configuration, has a cysteine–cysteine distance of ∼4.3 Å (Supplementary Fig. S3). Chain *D* in our structure has some unmodelled difference density around Cys312. It is plausible that chain *D* exists in mixed partial occupancy states whereby a minor fraction of the *D* chains have a reduced configuration. The formation of the disulfide bridge does not cause any large-scale changes in the overall arrangement of the structure, as shown by a superposition of chain *A* of our structure (PDB entry 4nct) with chain *A* from PDB entries 2vx3 and 3anq. However, it locks the N-terminal portion of the activation segment into a more rigid conformation, displacing residue Cys312 towards the catalytic motif HCD (Fig. 3). The rest of the activation loop is folded differently but is most likely to adopt multiple conformations, which in turn are likely to be influenced by the crystal packing. The DYRK1A structures complexed with INDY and harmine (PDB entries 3anq and 3anr), which have the same crystal packing (space group 19; $P2_12_12_1$) as PDB entry 4nct also have almost identical loop conformations after Cys312. However, details of the local fold
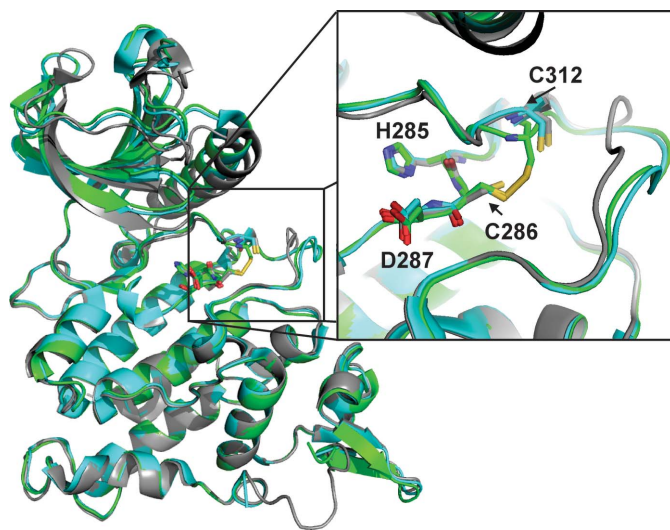

Figure 3
The structure reported here of DYRK1A (PDB entry 4nct) in complex with PKC412 (green) is superimposed with the published DYRK1A structures with PDB codes 2vx3 (grey) and 3anq (turquoise). The box highlights the disulfide bridge formed between Cys286 and Cys312 in DYRK1A in complex with PKC412 (green), which is absent in the 2vx3 and 3anq structures.

Table 2
Thermal shift experiments with DYRK1A and the inhibitors PKC412 and harmine.

Compound	Melting point, T_m (°C)
—	51
DMSO	51
PKC412	53
Harmine	57

Table 3
K_m and V_{max} from the kinetic assay.

	$K_{m(ATP)}$ (μM)	V_{max} (AU s^{-1})
DYRK1A	118.5 ± 7.8	51.5 ± 1.0
DYRK1B	80.7 ± 2.7	100.7 ± 0.9

around Cys312 differ compared with PDB entry 4nct, as the two previously published structures lack the disulfide bridge.

The HCD motif is rather rigid in the DYRK1A structure and is not significantly displaced upon disulfide-bridge formation (compared with the previously described structures). In contrast, the DFG motif and subsequent residues are displaced by 1–2 Å, with Cys312 moving most (almost 3 Å). In addition, the main-chain dihedrals between Ser311 and Cys312 change significantly (Fig. 4). Besides the displacement of activation-loop residues, formation of the disulfide induces changes in the local hydrogen-bonding network of the catalytic loop residues I^{283}IHCD^{287} and the activation-loop residues D^{307}FGSSCQ^{313}. The hydrogen bond between the backbone carbonyl of Ile284 and the backbone amide of Cys312 is weakened, and increases in length from 3.1 to 3.4 Å (Fig. 4). Analogously, the hydrogen bond between the backbone amide of Ile284 and the backbone carbonyl of Cys312 is lengthened by ~20% from 2.8 to 3.3 Å. The hydrogen bond between the side-chain OH of Ser311 and the carbonyl of His285 remains largely unchanged.

The HCD motif in the catalytic loop in DYRK kinases is rare in the human kinome. Besides the DYRK family, a cysteine in this position is found in only a few other kinases: the PKD family and the tyrosine-protein kinases SgK269, ULK4 and LRRK1 (ULK4 and LRRK1 have an FCD motif). Of these kinases, only UKL4 has a potential partner cysteine in the activation segment (between the DFG and APE motifs). The PKD kinases have no cysteine in the activation segment but they share a cysteine immediately preceding DFG, resulting in a conserved CDFG motif. However, any disulfide-bridge formation between this cysteine and other cysteines within the kinase domain would require additional reorganization of the fold.

3.4. Binding studies: thermal shift experiments

To further characterize the crystal structure, we tested the inhibition and binding of PKC412 *in vitro*. Thermal stabilization of a native protein upon ligand binding is a fast and robust way to screen for inhibitors, since the stabilizing effect of a compound upon binding can, to a first approximation, be proportional to the affinity and inhibitor concentration (Fedorov *et al.*, 2012). A thermal shift assay was performed to test the effect of PKC412 binding on the stability of DYRK1A undergoing thermal denaturation. Three parallel denaturation experiments were performed: DYRK1A in buffer, with DMSO and with PKC412 dissolved in DMSO. As a positive control, the published inhibitor harmine was used at the same

concentration in DMSO. The results are summarized in Table 2. The melting point for DYRK1A in buffer was 51°C. The addition of DMSO did not have any effect on the melting temperature, whereas the presence of PKC412 increased the melting point by 2°C. Interestingly, the smaller inhibitor harmine increased the melting temperature by around 6°C. PKC412 only forms hydrogen bonds at the hinge region, whereas harmine forms one hydrogen bond at the hinge and one to the catalytic Lys188 (Ogawa *et al.*, 2010). The binding of PKC412 is more predominantly hydrophobic in character. In addition, harmine is much more soluble in water than PKC412. Since the stabilizing effect of a compound is dependent on the extent of binding, and therefore on the concentration of the compound, the low solubility and therefore concentration of PKC412 in water could be the reason for the lower stabilizing effect compared with harmine. Although these approximations of linear dependence are observed to be valid in many cases, exceptions include destabilization upon (*i.e.* despite) binding, and the values for the thermal shifts must be interpreted with caution (Cimmperman *et al.*, 2008).

3.5. Activity assay: DYRK1A *versus* DYRK1B

PKC412 was further tested for its ability to inhibit the kinase activity of DYRK1A and DYRK1B *in vitro*. DYRK1B is the closest homologue of DYRK1A, with a sequence identity of about 85% for the kinase domain. An ATP-regenerative, NADH-consuming assay for kinases (Cook *et al.*, 1982) was used to determine the substrate-dependent
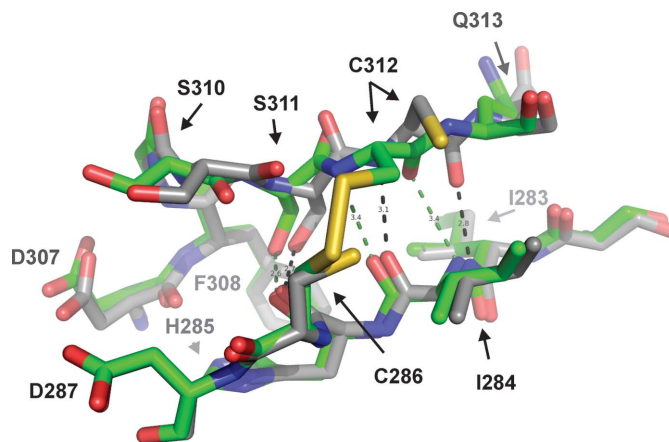

Figure 4
Superposition of chain *A* of PDB entry 4nct (green) with chain *A* of PDB entry 2vx3 (grey) showing the hydrogen-bond network between the catalytic loop and the activation loop. Formation of the disulfide bridge weakens the hydrogen interactions. The main change is the displacement of Cys312 and the neighbouring residues (Ser310–Gln313), while Cys286 and the HCD motif remain largely unchanged.

Michaelis–Menten constants for the kinase domains of DYRK1A and DYRK1B. The 15-residue peptide DYRKtide (RRRFRPASPLRGPPK) was used as a substrate for DYRK1A/B. The experiments were performed at room temperature in triplicate for a series of dilutions of ATP in the range from 50 mM to 4 µM (Fig. 5). The results of the K_m determination are summarized in Table 3. The K_m values for DYRK1A and DYRK1B are 118 and 80 µM, respectively, thus showing DYRK1B to have a somewhat stronger affinity for ATP in this assay and under these conditions. The K_m value for DYRK1A measured in the Cook assay is higher compared with the published value of ∼35 µM determined by a radiometric method (Himpel *et al.*, 2000). However, since the assay itself and the conditions, including temperature, substrate and kinase (full length *versus* kinase domain) used to determine the K_m values are different, differences are not unexpected. K_m values are sensitive to the specific assay conditions and K_m values for a single kinase do show variations (typically within a factor of five or less) when measured under different conditions (Knight & Shokat, 2005).

Table 4
IC_{50} and K_i values for PKC412 inhibition of DYRK1A and DYRK1B.

Kinase	ATP (µM)	IC_{50} (nM)	K_i (nM)
DYRK1A	128	59	28.4
DYRK1B	128	66	25.4

The Cook assay was used to quantify PKC412 inhibition of DYRK1A and DYRK1B (Fig. 6). PKC412 inhibits DYRK1A with an IC_{50} of 59 nM (at a constant ATP concentration of 128 µM), corresponding to a K_i of 28 nM [$K_{m(ATP)}$ = 118 µM]. PKC412 inhibits DYRK1B with a similar strength: the measured IC_{50} was 66 nM (at 128 µM ATP), with a resultant K_i of 25 nM [$K_{m(ATP)}$ = 80 µM]. These values are summarized in Table 4. For comparison, the K_i values determined under these assay conditions for harmine for DYRK1A and DYRK1B are 120 and 340 nM, respectively.

Under these assay conditions, PKC412 is thus equipotent against DYRK1A and DYRK1B. These DYRKtide phosphorylation assay results differ considerably from the K_d
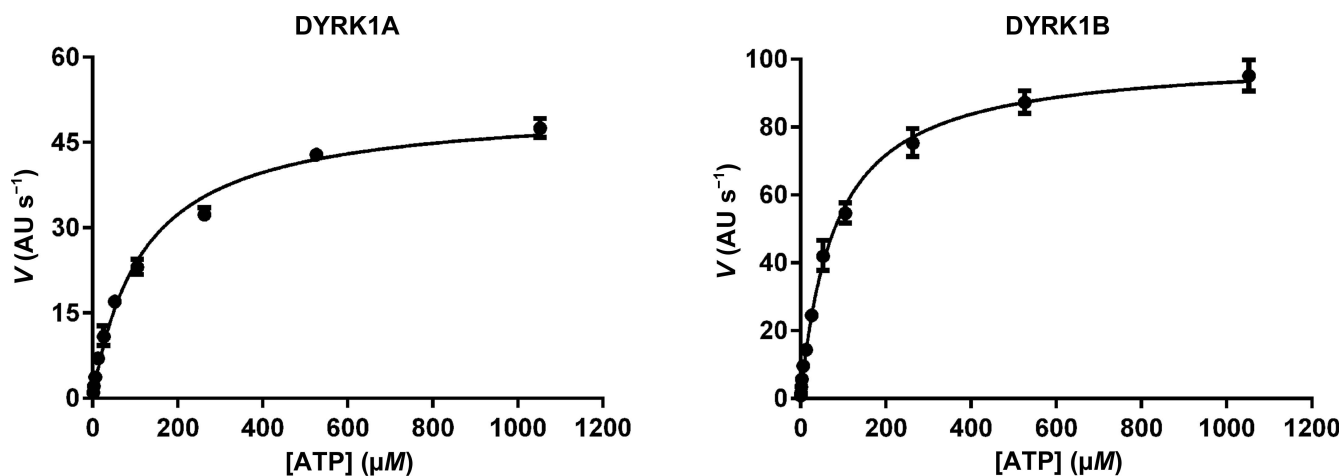

Figure 5
Michaelis–Menten plots to determine the K_m values for ATP. The concentration of the enzyme and the second substrate peptide DYRKtide were kept constant.
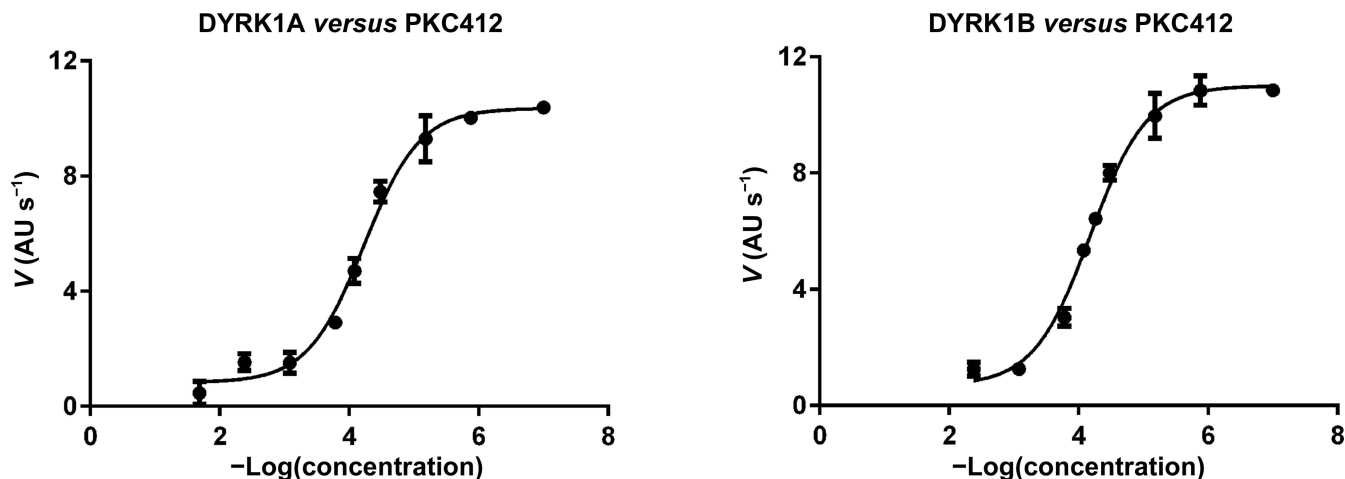

Figure 6
Dose–response curves for the inhibitor PKC412.

values published previously (Davis *et al.*, 2011). However, those values were determined in the absence of peptide substrate using different assay conditions. The relatively small differences between the affinities of PKC412 for DYRK1A *versus* DYRK1B are consistent with the fact that the two kinases differ by only one residue in the ATP pocket, namely methionine and leucine in DYRK1A and DYRK1B, respectively, at the gatekeeper +2 position at the hinge.

4. Discussion

One phenomenon that reflects alterations in the cellular redox environment is the extent of reversible modification of the thiol group in cysteine side chains (Groitl & Jakob, 2014). Redox-sensitive proteins play roles in all kinds of cellular signalling processes and include a growing list of protein kinases such as PDGFR, EGFR, IRK, FGFR, JAK, PKB, PKC, PKG, ASK1, MEKK1, MKK6, p38, c-Src, LYN, IKK, ATM and PKM2 (Giorgi *et al.*, 2010; Corcoran & Cotter, 2013; Truong & Carroll, 2013). Some of these proteins undergo reversible disulfide-bond formation in response to the redox status of the cell, which may alter signalling to rapidly adapt cellular processes. The disulfide bridge in DYRK kinases involves a cysteine located at a position in the catalytic loop which is otherwise highly conserved among protein kinases as an arginine. Johnson and coworkers defined the term 'RD kinase' after they observed that all kinases regulated through activation-loop phosphorylation have a conserved arginine immediately preceding the conserved catalytic aspartate in the HRDLK*xx*N (or HRD) motif of the catalytic loop (Johnson *et al.*, 1996). The HRD arginine anchors the phosphate group of the primary phosphorylation site of the activation loop, stabilizing it in an active conformation (Nolen *et al.*, 2004). The location of Cys286 as a substitution for the HRD arginine is a rare but distinguishing feature of DYRK-family kinases. Both Cys286 and Cys312 are located in positions corresponding to the RD pocket. It is reasonable to hypothesize that the cysteines in such a strategic location can act as a redox-sensitive switch, much as RD kinases (ex ERKs) are regulated by an electrostatic phosphorylation switch. Others have previously proposed redox regulation as a potential mode of regulation for DYRK family kinases (Becker & Joost, 1999; Becker & Sippl, 2011; Kannan & Neuwald, 2004). Becker and Sippl pointed out that the thiol moieties of these cysteines were sufficiently close (∼4.3 Å in DYRK1A and DYRK2) to allow the formation of a disulfide bridge. They further speculated that the potential switch between —SH reduced and —S—S— oxidized states could result in a conformational change and altered catalytic activity of DYRK kinases (Becker & Sippl, 2011). This followed an earlier proposal based on homology modeling that the formation of a disulfide bond between Cys286 and Cys312 might stabilize the activation loop (Kannan & Neuwald, 2004). The structure that we present in this work confirms the occurrence of this disulfide bond and demonstrates a role in the stabilization of the activation segment: the covalent disulfide bond holds the activation loop near the catalytic loop in a conformation altered relative to

that of the unbound activation loop. Thus, one function of DYRK1A (and the other DYRK family members) might be to sense the presence of reactive oxygen species (ROS): an increasingly oxidizing environment would induce the formation of the disulfide bridge and trigger a signalling response. In this context, it is interesting to note that DYRK1B (the closest related kinase to DYRK1A) plays a role in the regulation of ROS levels. In quiescent cultures of pancreatic SU86.86 and Panc1 cancer cells, DYRK1B reduced the levels of ROS by increasing the transcription of the antioxidant genes ferroxidase, superoxide dismutase SOD2 and SOD3 (Deng *et al.*, 2009, 2014).

PKC412 (midostaurin) is in phase III clinical trials to treat acute myeloid leukaemia; a possible application in neurological disease has not been established. However, the structure of DYRK1A–PKC412, together with characterization of the binding, may aid in the consideration of alternate uses of PKC412 or its derivatives in which DYRK kinases represent the main target or targets. Potentially relevant diseases for such expanded applications include neurological diseases such as Alzheimer's or Down syndrome.

References

Adams, P. D. *et al.* (2010). *Acta Cryst.* D**66**, 213–221.
Anderson, K. *et al.* (2013). *Bioorg. Med. Chem. Lett.* **23**, 6610–6615.
Aranda, S., Laguna, A. & de la Luna, S. (2011). *FASEB J.* **25**, 449–462.
Becker, W. & Joost, H. G. (1999). *Prog. Nucleic Acid Res. Mol. Biol.* **62**, 1–17.
Becker, W. & Sippl, W. (2011). *FEBS J.* **278**, 246–256.
Becker, W., Soppa, U. & Tejedor, F. J. (2014). *CNS Neurol. Disord. Drug Targets*, **13**, 26–33.
Becker, W., Weber, Y., Wetzel, K., Eirmbter, K., Tejedor, F. J. & Joost, H. G. (1998). *J. Biol. Chem.* **273**, 25893–25902.
Bubnoff, N. von, Engh, R. A., Aberg, E., Sänger, J., Peschel, C. & Duyster, J. (2009). *Cancer Res.* **69**, 3032–3041.
Cimmperman, P., Baranauskienė, L., Jachimovičiūtė, S., Jachno, J., Torresan, J., Michailovienė, V., Matulienė, J., Sereikaitė, J., Bumelis, V. & Matulis, D. (2008). *Biophys. J.* **95**, 3222–3231.
ClinicalTrials (2014). *Daunorubicin, Cytarabine, and Midostaurin in Treating Patients With Newly Diagnosed Acute Myeloid Leukemia.* http://www.clinicaltrials.gov/show/NCT00651261.
Cook, P. F., Neville, M. E. Jr, Vrana, K. E., Hartl, F. T. & Roskoski, R. Jr (1982). *Biochemistry*, **21**, 5794–5799.
Corcoran, A. & Cotter, T. G. (2013). *FEBS J.* **280**, 1944–1965.
Davis, M. I., Hunt, J. P., Herrgard, S., Ciceri, P., Wodicka, L. M., Pallares, G., Hocker, M., Treiber, D. K. & Zarrinkar, P. P. (2011). *Nature Biotechnol.* **29**, 1046–1051.
Deng, X., Ewton, D. Z. & Friedman, E. (2009). *Cancer Res.* **69**, 3317–3324.
Deng, X., Ewton, D. Z., Pawlikowski, B., Maimone, M. & Friedman, E. (2003). *J. Biol. Chem.* **278**, 41347–41354.

Deng, X., Mercer, S. E., Sun, C.-Y. & Friedman, E. (2014). *Genes Cancer*, **5**, 22–30.

Diao, Y., Liu, W., Wong, C. C. L., Wang, X., Lee, K., Cheung, P.-Y., Pan, L., Xu, T., Han, J., Yates, J. R. III, Zhang, M. & Wu, Z. (2010). *Proc. Natl Acad. Sci. USA*, **107**, 20974–20979.

Eaton, P. (2006). *Free Radic. Biol. Med.* **40**, 1889–1899.

Emsley, P., Lohkamp, B., Scott, W. G. & Cowtan, K. (2010). *Acta Cryst.* D**66**, 486–501.

Evans, P. (2012). *Science*, **336**, 986–987.

Fabbro, D., Ruetz, S., Bodis, S., Pruschy, M., Csermak, K., Man, A., Campochiaro, P., Wood, J., O'Reilly, T. & Meyer, T. (2000). *Anticancer Drug. Des.* **15**, 17–28.

Fedorov, O., Niesen, F. H. & Knapp, S. (2012). *Methods Mol. Biol.* **795**, 109–118.

Fischer, T. *et al.* (2010). *J. Clin. Oncol.* **28**, 4339–4345.

Friedman, E. (2010). *Cancers (Basel)*, **2**, 1492–1512.

Friedman, E. (2013). *Int. J. Mol. Sci.* **14**, 5560–5575.

Gani, O. A. & Engh, R. A. (2010). *Nat. Prod. Rep.* **27**, 489–498.

Giorgi, C., Agnoletto, C., Baldini, C., Bononi, A., Bonora, M., Marchi, S., Missiroli, S., Patergnani, S., Poletti, F., Rimessi, A., Zavan, B. & Pinton, P. (2010). *Antioxid. Redox Signal.* **13**, 1051–1085.

Griffith, J., Black, J., Faerman, C., Swenson, L., Wynn, M., Lu, F., Lippke, J. & Saxena, K. (2004). *Mol. Cell*, **13**, 169–178.

Groitl, B. & Jakob, U. (2014). *Biochim. Biophys. Acta*, **1844**, 1335–1343.

Guimerá, J., Casas, C., Pucharcòs, C., Solans, A., Domènech, A., Planas, A. M., Ashley, J., Lovett, M., Estivill, X. & Pritchard, M. A. (1996). *Hum. Mol. Genet.* **5**, 1305–1310.

Himpel, S., Tegge, W., Frank, R., Leder, S., Joost, H. G. & Becker, W. (2000). *J. Biol. Chem.* **275**, 2431–2438.

Ionescu, A., Dufrasne, F., Gelbcke, M., Jabin, I., Kiss, R. & Lamoral-Theys, D. (2012). *Mini Rev. Med. Chem.* **12**, 1315–1329.

Janel, N. *et al.* (2014). *Transl. Psychiatr.* **4**, e425.

Johnson, L. N., Noble, M. E. M. & Owen, D. J. (1996). *Cell*, **85**, 149–158.

Kang, J. E., Choi, S. A., Park, J. B. & Chung, K. C. (2005). *J. Neurosci. Res.* **81**, 62–72.

Kannan, N. & Neuwald, A. F. (2004). *Protein Sci.* **13**, 2059–2077.

Karplus, P. A. & Diederichs, K. (2012). *Science*, **336**, 1030–1033.

Kim, E. J., Sung, J. Y., Lee, H. J., Rhim, H., Hasegawa, M., Iwatsubo, T., Min, D. S., Kim, J., Paik, S. R. & Chung, K. C. (2006). *J. Biol. Chem.* **281**, 33250–33257.

Knight, Z. A. & Shokat, K. M. (2005). *Chem. Biol.* **12**, 621–637.

Krug, M., Weiss, M. S., Heinemann, U. & Mueller, U. (2012). *J. Appl. Cryst.* **45**, 568–572.

Liu, F., Liang, Z., Wegiel, J., Hwang, Y.-W., Iqbal, K., Grundke-Iqbal, I., Ramakrishna, N. & Gong, C.-X. (2008). *FASEB J.* **22**, 3224–3233.

Manning, G., Whyte, D. B., Martinez, R., Hunter, T. & Sudarsanam, S. (2002). *Science*, **298**, 1912–1934.

McCoy, A. J., Grosse-Kunstleve, R. W., Adams, P. D., Winn, M. D., Storoni, L. C. & Read, R. J. (2007). *J. Appl. Cryst.* **40**, 658–674.

Murshudov, G. N., Skubák, P., Lebedev, A. A., Pannu, N. S., Steiner, R. A., Nicholls, R. A., Winn, M. D., Long, F. & Vagin, A. A. (2011). *Acta Cryst.* D**67**, 355–367.

Nolen, B., Taylor, S. & Ghosh, G. (2004). *Mol. Cell*, **15**, 661–675.

Ogawa, Y., Nonaka, Y., Goto, T., Ohnishi, E., Hiramatsu, T., Kii, I., Yoshida, M., Ikura, T., Onogi, H., Shibuya, H., Hosoya, T., Ito, N. & Hagiwara, M. (2010). *Nature Commun.* **1**, 86.

Omura, S., Iwai, Y., Hirano, A., Nakagawa, A., Awaya, J., Tsuchiya, H., Takahashi, Y. & Asuma, R. (1977). *J. Antibiot.* **30**, 275–282.

Park, J., Song, W.-J. & Chung, K. C. (2009). *Cell. Mol. Life Sci.* **66**, 3235–3240.

Prade, L., Engh, R. A., Girod, A., Kinzel, V., Huber, R. & Bossemeyer, D. (1997). *Structure*, **5**, 1627–1637.

Schüttelkopf, A. W. & van Aalten, D. M. F. (2004). *Acta Cryst.* D**60**, 1355–1363.

Smith, B., Medda, F., Gokhale, V., Dunckley, T. & Hulme, C. (2012). *ACS Chem. Neurosci.* **3**, 857–872.

Soundararajan, M., Roos, A. K., Savitsky, P., Filippakopoulos, P., Kettenbach, A. N., Olsen, J. V., Gerber, S. A., Eswaran, J., Knapp, S. & Elkins, J. M. (2013). *Structure*, **21**, 986–996.

Stone, R. M., Fischer, T., Paquette, R., Schiller, G., Schiffer, C. A., Ehninger, G., Cortes, J., Kantarjian, H. M., DeAngelo, D. J., Huntsman-Labed, A., Dutreix, C., del Corral, A. & Giles, F. (2012). *Leukemia*, **26**, 2061–2068.

Tahtouh, T. *et al.* (2012). *J. Med. Chem.* **55**, 9312–9330.

Teipel, S. J. & Hampel, H. (2006). *Behav. Genet.* **36**, 405–415.

Thies, W. & Bleiler, L. (2012). *Alzheimers Dement.* **8**, 131–168.

Truong, T. H. & Carroll, K. S. (2013). *Crit. Rev. Biochem. Mol. Biol.* **48**, 332–356.

Walte, A., Rüben, K., Birner-Gruenberger, R., Preisinger, C., Bamberg-Lemper, S., Hilz, N., Bracher, F. & Becker, W. (2013). *FEBS J.* **280**, 4495–4511.

Weisberg, E., Boulton, C., Kelly, L. M., Manley, P., Fabbro, D., Meyer, T., Gilliland, D. G. & Griffin, J. D. (2002). *Cancer Cell*, **1**, 433–443.

Winn, M. D. *et al.* (2011). *Acta Cryst.* D**67**, 235–242.

Woods, Y. L., Cohen, P., Becker, W., Jakes, R., Goedert, M., Wang, X. & Proud, C. G. (2001). *Biochem. J.* **355**, 609–615.